Hydrometallurgy 222 (2023) 106192

Contents lists available at ScienceDirect

Hydrometallurgy

journal homepage: www.elsevier.com/locate/hydromet

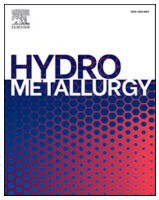

Recycling of NdFeB magnets: Model supported iron minimization via in-situ hydrolysis during leaching and hematite precipitation in an autoclave

Elif Emil-Kaya [a,b,c,*], Ozan Kaya [d], Srecko Stopic [b], Sebahattin Gürmen [c], Bernd Friedrich [b]

[a] Department of Materials Science and Eng., Norwegian University of Science and Technology, 7034 Trondheim, Norway
[b] IME Process Metallurgy and Metal Recycling, RWTH Aachen University, 52056 Aachen, Germany
[c] Department of Metallurgical & Materials Eng., Istanbul Technical University, 34469 Istanbul, Türkiye
[d] Department of Mechatronics Eng., Istanbul Technical University, 34469 Istanbul, Türkiye

ARTICLE INFO

Keywords:
NdFeB recycling
Rare earth elements
iron hydrolysis
Hematite precipitation
Autoclave

ABSTRACT

The NdFeB magnets are a significant component of technological applications, which contain a remarkable quantity of rare earth elements (REEs). For this reason, the recycling of NdFeB magnets is essential for the reuse of these elements. This research represents the recycling strategy of NdFeB magnets, which consists of iron minimization through in-situ hydrolysis during oxidative leaching and hematite precipitation in an autoclave. The influence of the experimental parameters in the hydrolysis of Fe^{3+} in a nitric acid medium on the formation of a mixture of iron oxide hydroxide was examined in detail. Afterward, the effect of the temperature, time and, water addition on the iron and REEs precipitation in the autoclave was investigated by the ANOVA analysis based on the Box-Behnken design. According to the particle swarm optimization algorithm, maximum REEs extraction and minimum iron extraction were achieved in a solution of 1.82 mol/L nitric acid, at a solid/liquid ratio of 11/100, a temperature of 60 °C, and a stirring speed of 415 rpm. The mean leaching efficiencies of REEs and iron are calculated to be 76% and 7%, respectively. The optimal parameters for hematite precipitation in the autoclave were determined to be a process temperature of approximately 137 °C, a processing time of approximately 3 h and 55 min, and a water addition of approximately 20%. The optimum parameters are in harmony with the validation experiments.

1. Introduction

Worldwide demand for rare earth elements (REEs) has increased strongly due to the utilization of these elements in high-tech products, including permanent magnets, phosphorus materials, catalysts, and batteries. Increasing concerns about REEs supply and environmental problems in ore production, limited resources, and national policies have led to an increase in studies about the recovery of REEs from scrap materials (Rim, 2016; Lewicka et al., 2021; Mudali et al., 2021). The NdFeB magnets which contain up to 30% REEs (Nd, Pr, and Dy) are one of the most remarkable scraps for the recovery since the content of REEs in magnets is higher than in some REEs-bearing minerals (Zhang et al., 2020a, 2020b; Barkov et al., 2021; Tay et al., 2021). In the literature, there has been an abundance of research on the recovery of REEs based on pyrometallurgy and hydrometallurgy (Kruse et al., 2017; Chung et al., 2022; Polyakov and Sibilev, 2015; Stopic et al., 2022; Kaya et al., 2021; Omodara et al., 2019; Böhm et al., 2023; Ilatovskaia et al., 2023). Hydrometallurgy is the widely preferred technique for the extraction of REEs from scrap materials. Lower grade and complex streams can be conducted by hydrometallurgical routes eventuated in high product purity (Akcil et al., 2021; Tunsu et al., 2016; Peelman et al., 2016; Emil-Kaya et al., 2022; Uysal et al., 2022; Du et al., 2023.).

Selective precipitation processes have been performed for REEs extraction, after the direct leaching process of NdFeB magnets. Tian et al. (2019) leached NdFeB magnet powders with HCl. They used hexamethylenetetramine (HMTA) and tartaric acid as chelating agents to prevent iron precipitation during the leaching process. In another study, NdFeB magnet powders were leached with HCl, and the conversion of Fe^{2+} to Fe^{3+} was performed by electrochemical method. The purity of RE oxides obtained by precipitation with oxalic acid following the calcination process was 99.2% (Venkatesan et al., 2018). As an alternative to the chemical conversion of iron, Parhi et al. (2016) preferred to use H_2O_2 to oxidize Fe^{2+} to Fe^{3+} after the leaching process with HCl. The HNO_3 leaching with the addition of H_2O_2 has also been

* Corrresponding author at: Department of Materials Science and Eng., Norwegian University of Science and Technology, 7034 Trondheim, Norway.
E-mail address: elif.e.kaya@ntnu.no (E. Emil-Kaya).

https://doi.org/10.1016/j.hydromet.2023.106192
Received 25 July 2022; Received in revised form 14 September 2023; Accepted 16 September 2023
Available online 27 September 2023

investigated. Iron was precipitated as $Fe(OH)_3$ by adjusting the pH to 3 using NaOH. Subsequent use of oxalic acid as a precipitation agent resulted RE oxides of 68% purity (Rabatho et al., 2013). Likewise, the recycling of NdFeB magnets was performed by complete leaching with iron removal using MnO_2 for chemical oxidation of Fe^{2+} to Fe^{3+} (Önal et al., 2017). As a different process, NdFeB magnet powders were leached with mineral acid including HCl, H_2SO_4, and HNO_3 without the addition of a chemical agent for the conversion of iron. Following that, selective iron precipitation was carried out in a hydrothermal reactor in two steps with the addition of glucose which provided the hydrolysis of Fe^{3+} into hematite without losing REEs (Lin et al., 2019).

Hematite precipitation in an autoclave is a well-known process, but still needs to be investigated for recycling of NdFeB. It was reported that the hematite precipitation from ferric chloride at a temperature <100 °C at atmospheric pressure, where β-FeO.OH was formed at approximately 60 °C by controlling the seeding and changing the molarity of the solution. Prolonged retention time favored a stable hematite phase, at times longer than 100 h only the hematite phase was observed (Dutrizac and Riveros, 1999). In the zinc industry, the hematite precipitation process has been employed for the iron removal process. The kinetics and chemistry of the hematite precipitation were elucidated. In their study, hematite was formed through the oxydrolysis reaction of ferrous sulphate at temperatures of between 195 and 200 °C at a pressure in the range of 103 to 414 kPa (Cheng et al., 2003). In another study, the precipitation kinetic of ferric sulphate in a batch reactor at 200 °C was investigated. The hematite precipitate with various formulas was obtained by manipulating process conditions such as the absence/presence of zinc sulphate and Fe^{+3} concentration (Cheng and Demopoulos, 2004). In another study, the hematite precipitation was accomplished from a ferric chloride solution in an autoclave. The precipitation of hematite was achieved at approximately 100 °C in the presence of hematite seed (Riveros and Dutrizac, 1997).

Since the interaction among the parameters and defining optiormmum process conditions via the conventional technique could not be accomplished, the statistical experimental design methods such as Taguchi and Box-Behnken methods were preferred in many studies, to determine optimum process parameters and their relationship with each other (Unal and Kaya, 2020; Wang et al., 2011; Dutta et al., 2021). In recent years, experimental design techniques have been frequently used in hydrometallurgical studies for the determination of optimum leaching parameters (Dahasahastra et al., 2022; Pan et al., 2020; Zhang et al., 2020a, 2020b; Yazici and Deveci, 2013). In particular, Taguchi's experimental design effectively reduces the number of experiments for identifying the optimal process parameters. Subsequently, ANOVA analysis assigns the significant leaching process parameters. However, experimental design techniques allow a single objective to be achieved. In case of multiple objectives in the process, optimization methods can define optimum process conditions. Among them, particle swarm optimization (PSO) has attracted attention due to it being conveniently implemented in various fields (Robinson and Rahmat-Samii, 2004; Coello et al., 2004). With experimental design methods such as Taguchi and Box Behnken and optimization methods, including PSO, optimum experimental parameters can be defined with a small number of experiments.

In this study, oxidative leaching is developed for iron removal by favoring in-situ iron hydrolysis during oxidative leaching for the first time. To define maximum REEs and minimum iron dissolution during leaching, the leaching experiments are performed based on Taguchi orthogonal array. Afterward, maximum REEs and minimum iron dissolution are determined by the PSO method. Hematite precipitation in an autoclave is a well-known process, however, systematic study of hematite precipitation in an autoclave for the recycling of NdFeB magnets is still outstanding. Following the oxidative leaching, the dissolved iron was precipitated in the autoclave under pressure and temperature based on the Box-Behnken experimental design.

Table 1
Oxidative leaching parameters and their levels for NdFeB magnets.

Parameters		Levels		
		1	2	3
Acid Concentration	mol/L	1	2	3
Solid: Liquid Ratio	*w/v*	1/10	1/20	1/30
Temperature	°C	40	60	80
Stirring Speed	rpm	200	350	500

2. Material and method

2.1. Experimental design of leaching process by Taguchi method

Firstly, a preliminary leaching experiment was performed for 120 min. Samples were collected for chemical analysis every 15 min. Since there was no significant increase in dissolution amounts of elements after 30 min, the leaching time of 30 min was chosen. Taguchi orthogonal array (L9) approach was applied for the experimental design of the leaching process. The solid/liquid ratio was varied in three levels of 1/10, 1/20, and 1/30, the reaction temperature was adjusted in three levels of 40, 60, and 80 °C, and the stirring rate was adjusted in three levels of 200, 350, and 500 rpm. Table 1 shows the oxidative leaching parameters.

2.2. Scrap NdFeB magnet powders characterization and methodology for leaching experiments

Scrap NdFeB magnets were supplied in bulk form. The NdFeB magnets were crushed by a jaw crusher (Retsch GmbH, Haan, Germany). The chemical composition of the magnet powders was determined using X-ray fluorescence (XRF) spectroscopy (Panalytical WDXRF spectrometer, Malvern Panalytical B.*V*., Eindhoven, Netherlands). Afterward, NdFeB magnet powders were dissolved in a solution of 3 mol/L nitric acid to define the detailed chemical composition of the NdFeB magnet. After solid/liquid separation by vacuum filtration setup, this solution was analyzed by inductively coupled plasma optical emission spectroscopy (ICP-OES) (SPECTRO ARCOS, SPECTRO Analytical Instruments GmbH, Kleve, Germany). The phase analysis of NdFeB magnet powders was revealed by X-ray Diffractometer (Bruker D8 Advance) with a LynxEye detector using Cu—K radiation (λ = 1.54187 Å). Particle size distribution of NdFeB magnet powders was revealed by a dynamic particle analyzer with an M5 lens (SympaTech QuickPick Oasis).

Leaching experiments were performed in a 1000 mL three-neck round bottom glass flask with 200 mL diluted nitric acid. Nitric acid (65%) was provided from VWR International GmbH, Darmstadt, Germany. The heating mantle (IKA Werke GmbH, Staufen in Breisgau, Germany) was used to control the temperature of the experiment. The slurry in the flask was agitated with a mechanical stirrer at various speeds for 30 min. The experimental setup for leaching was reported elsewhere (Emil-Kaya et al., 2023).

A vacuum filtration setup was utilized to separate the leaching solution and the leach residue. The leaching behavior of metals was evaluated by ICP-OES. Potentiometric titration of Fe^{2+} in the leaching solution was conducted with cerium(IV) sulfate by titration system (Metrohm Dosimat 655, Titrosampler 855).

X-ray diffraction analysis (XRD) revealed the phase content of the leach residue and the calcined leach residue (Bruker D8 Advance with LynxEye detector). The XRD patterns of the calcined leach residue and the leach residue were recorded in the 2θ range of 10–90°. The morphological investigation of the leach residue was performed by Scanning Electron Microscope (SEM, Zeiss Gemini 500). Moreover, the elemental composition of the leach residue was revealed by Energy Dispersive Spectroscopy (EDS). Fourier-Transform infrared spectrum of the leach residue was recorded between 4000 and 400 cm^{-1} by Fourier-Transform infrared spectroscopy (FTIR, Bruker Alpha T).

Table 2
Process parameters and their levels for Box-Behnken Design.

Parameters	Levels		
	1	2	3
Process Temperature (°C)	120	140	160
Time (h)	2	4	6
Water Addition (%)	0	25	50

2.3. Box Behnken design for iron precipitation process in the autoclave

This section investigated the effect of temperature and time on the recovery and removal efficiencies of REEs and iron, respectively. Temperature and precipitation time in an autoclave were reported as important parameters for iron precipitation in the literature (Lin et al., 2019; Dutrizac and Riveros, 1999; Cheng et al., 2003; Cheng and Demopoulos, 2004; Riveros and Dutrizac, 1997). The effect of water addition, which has not been investigated before in the literature, was also investigated in this section. Based on the idea that the addition of water increases the pH value, water was added to the leaching solution at certain rates, and the pH of the leaching solution was measured. The pH value of the solutions with water addition of 0%, 25%, and 50% was measured as 2.15, 2.24, and 2.31, respectively. Moreover, the effect of water addition on metal ion concentration and recovery (%) of REEs and the removal efficiency of iron (%) was investigated.

A Box-Behnken design was employed for the iron removal process in an autoclave under pressure. The precipitation experiments in the autoclave were conducted with three parameters at three levels. Process temperature was adjusted in three levels of 120, 140, and 160 °C, process time of 2, 4, and 6 h and water addition of 0, 25, and 50%. The process parameters and their levels can be found in Table 2.

2.4. Iron precipitation process in the autoclave

The precipitation studies were conducted in a 1500 mL autoclave (Büchi Kiloclave Type 3E, Switzerland) with 100 mL leach liquid at varied temperatures and durations. These experiments were carried out without the use of gas pressure. A water-cooling system was employed to cool the autoclave at the end of the experiment. A centrifuge was used to separate the precipitated hematite from the leach liquor. The precipitates were dried at 65 °C in the furnace. Afterward, the precipitates were analyzed by XRD analysis.

3. Results and discussion

3.1. Characterization of scrap NdFeB magnet powders

The composition of NdFeB magnet powders was determined using X-ray fluorescence analysis. Table 3 shows the phase composition of NdFeB magnet powders. The presence of Fe, Nd, and Pr, as well as small amounts of Tb, Al, Si, Co, Mn, and Pd, was detected with XRF analysis.

Table 3
The chemical composition of NdFeB magnet powders determined by XRF analysis.

Component	Fe_2O_3	Nd_2O_3	Pr_2O_3	MnO	Tb_4O_7
Concentration (wt%)	68.1	20.4	5.72	1.97	0.70
Component	**Co_3O_4**	**Al_2O_3**	**Na_2O**	**PdO**	**SiO_2**
Concentration (wt%)	0.70	0.42	0.34	0.24	0.24
Component	**As_2O_3**	**Ga_2O_3**	**CuO**	**Nb_2O_5**	**Other**
Concentration (wt%)	0.21	0.20	0.14	0.12	0.50

Table 4
Chemical analysis of NdFeB magnet powders determined by ICP analysis.

Composition	Fe	Nd	Pr	B	Co
Concentration (wt%)	66.3	23.9	7.38	0.877	0.773
Composition	**Dy**	**Cu**	**Mo**	**Cr**	**Ni**
Concentration (wt%)	0.662	0.102	< 0.1	< 0.1	< 0.1

The result of the ICP-OES analysis of NdFeB magnet powders is shown in Table 4.

The presence of Fe, Nd, and Pr, as well as small amounts of Cu, B, Co, and Dy, was detected with ICP analysis. The phase analysis of NdFeB magnet powders was performed by (XRD) analysis. Fig. 1. depicts the XRD pattern of the magnet powders.

The XRD peaks in the pattern of NdFeB magnet powders correspond to tetragonal structure $Nd_2Fe_{14}B$ with the space group of P42/mnm (JCPDS #40–1028). Fig. 2 shows an SEM image of NdFeB magnet particles.

The morphology of the NdFeB magnet powders was non-uniform, having a large size distribution. Furthermore, EDS analysis confirmed the presence of Nd, Fe, and Pr. Fig. 3 shows the dynamic particle analysis of NdFeB magnet powders.

Fig. 3 reveals the distribution density (q_3*) and the distribution sum (Q_3) of the NdFeB magnet powders with the diameter (EQPC)-value of the NdFeB magnet powders. According to the distribution sum (Q_3), the $d_{90.3}$, $d_{50.3}$, and $d_{10.3}$ values are 90.19 μm, 56.01 μm, and 11.50 μm, respectively. These results confirm that 90.3% of the NdFeB magnet powders have a grain size smaller than 90.2 μm. The distribution density of powders (q_3*) reaches its global maximum at ~80 μm.

3.2. Characterization of leach residue occurred through in-situ iron hydrolysis during leaching

$$Fe_{(s)} + 2HNO_3 \rightarrow Fe^{2+} + 2NO_2^- + 2OH^- \ (\Delta G^{o}_{60^{\circ}C} = -164.621\ kJ) \quad (1)$$

In the hydrometallurgical process, the nitric acid medium has several advantages, such as the ability to create highly oxidizing conditions and to use oxygen directly from air. This medium has unique properties in terms of iron oxidation. The removal of iron from the recycling process of the NdFeB magnet is an important step in producing high-purity RE oxides. Nitric acid promotes the oxidation of Fe^{2+} to Fe^{3+}. Chemical reactions occur during the leaching process when NdFeB magnet particles interact with nitric acid. These reactions (Eq. 1–5) are described as follows.

$$Fe_{(s)} + 3HNO_3 \rightarrow Fe^{3+} + 3NO_2^- + 3OH^- \ (\Delta G^{o}_{60^{\circ}C} = -143.769\ kJ) \quad (2)$$

$$Nd_{(s)} + 3HNO_3 \rightarrow Nd^{3+} + 3NO_2^- + 3OH^- \ (\Delta G^{o}_{60^{\circ}C} = -797.625\ kJ) \quad (3)$$

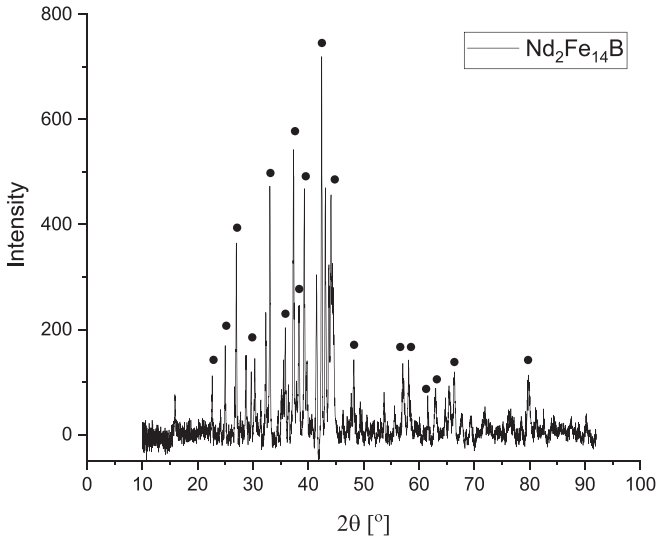

Fig. 1. X-ray diffraction analysis of NdFeB magnet powders.

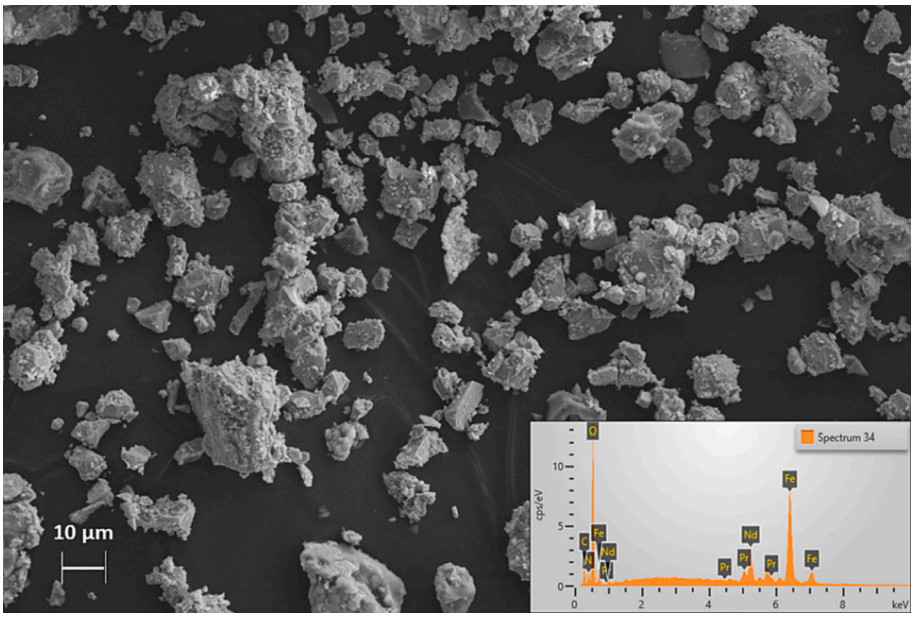

Fig. 2. SEM micrograph of NdFeB magnet powders.

$$Pr_{(s)} + 3HNO_3 \rightarrow Pr^{3+} + 3NO_2^- + 3OH^- \ (\Delta G^o_{60°C} = -788.947\ kJ) \quad (4)$$

$$Dy_{(s)} + HNO_3 \rightarrow Dy^{3+} + 3NO_2^- + 3OH^- \ (\Delta G^o_{60°C} = -793.874\ kJ) \quad (5)$$

Gibbs free energy calculations of the abovementioned equations at 60 °C were conducted in HSC Chemistry 9.

Hydrolysis of Fe^{3+} nitrate at high temperatures results in the formation of hematite and goethite. The precipitation behavior of dissolved Fe^{2+} differs from that of dissolved Fe^{3+}. While Fe^{2+} precipitates at the same pH level as REEs, Fe^{3+} precipitates at a lower pH level than Fe^{2+} and REEs with base media. Iron ions in the solution as Fe^{3+} enable the separation of REEs. Intending to determine the quantity of Fe^{2+} in the leach liquor, we performed the potentiometric titration analysis. The amount of Fe^{2+} in the leach liquors, which were performed with the specified condition, is <1%. The mean pH value was 2.15 for all validation experiments conducted under the specified conditions. This pH value favors the continuation of the hydrolysis of Fe after the completion of the leaching process. The NdFeB magnet powders initiate an exothermic reaction with nitric acid. The removal of iron via hydrolysis at high temperatures during the direct leaching process appears to be a simple solution for NdFeB recycling. During the leaching process, goethite and $Fe(OH)_{3(solid)}$ were formed through the Feitknecht reaction sequence, which enables the selective leaching of REEs. This reaction sequence (Eqs. 6–9) is described as follows (Feitknecht and Michaelis, 1962);

$$O_{2(g)} \rightleftharpoons O_{2(aq)} \quad (6)$$

$$Fe^{2+} + 2H_2O = Fe(OH)_2 + 2H^+ \quad (7)$$

$$Fe(OH)_2 + \frac{1}{4}O_2 + \frac{1}{2}H_2O = Fe(OH)_{3(solid)} \quad (8)$$

$$Fe(OH)_{3(solid)} = \alpha - FeOOH_{(solid)} + H_2O \quad (9)$$

The control experiment was conducted at 60 °C under the specified conditions. However, due to the exothermic reaction of NdFeB magnet powders and nitric acid, the reaction temperature was measured at >60 °C in the first 15 min. The graph was created with the x-axis representing the leaching time and the y-axis representing the leaching temperature. Fig. 4 shows the reaction temperature of magnet powders in nitric acid as a function of time.

The formation of goethite is favored by the high reaction temperature (Babjan, 1971). If the reaction occurs at a lower temperature, then the formation of $Fe(OH)_{3(solid)}$ is expected, and in this case, the

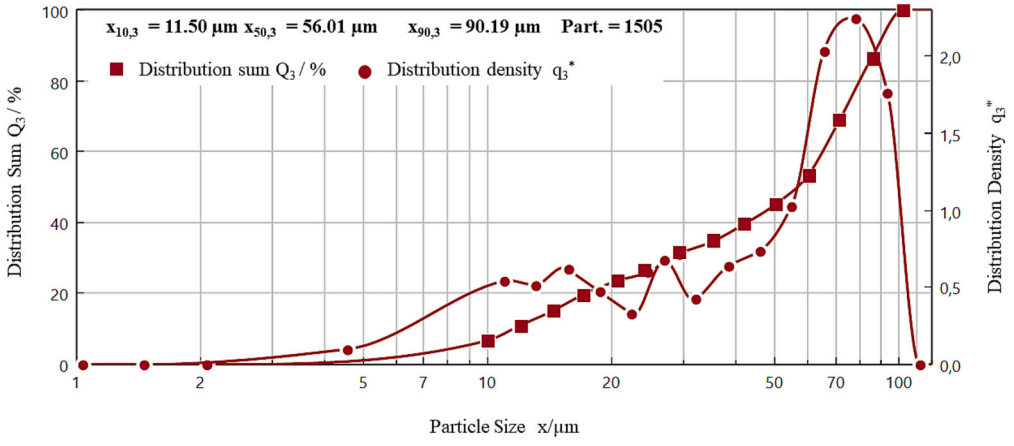

Fig. 3. Dynamic particle analysis of NdFeB magnet powders.

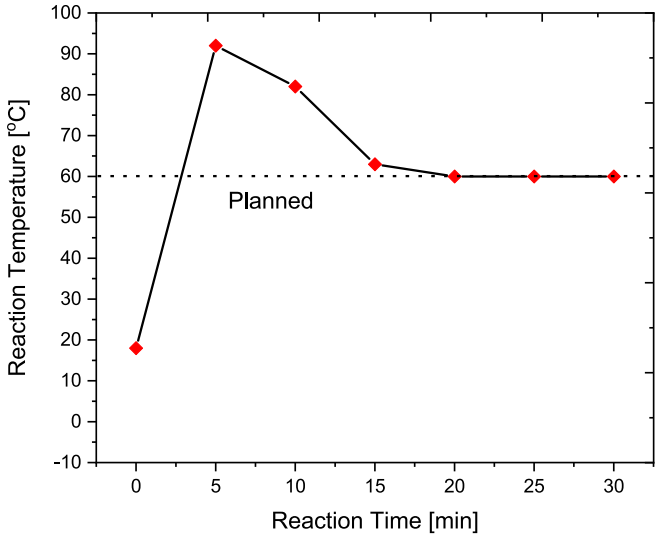

Fig. 4. Reaction temperature of magnet powders in nitric acid as a function of time.

formation of mixed amorphous goethite and $Fe(OH)_{3(solid)}$ is expected. Fig. 5 shows X-ray diffraction analyses of the leach residue and the calcined leach residue from the validation experiments.

The broad peak in the leach residue confirmed the amorphous form. The XRD peak at 38.10° corresponds to orthorhombic iron oxide hydroxide (PDF card No. 00–044-1415). The calcined residue was mainly Fe_2O_3 with a small amount of $NdFeO_3$ phase. The reflection lines (012), (104), (110), (113), (024), (116), (214), (300), and (1010) have been assigned to the peaks at $2\theta = 24.20°$, 33.23°, 35.70°, 40.95°, 49.57°, 54.20°, 62.58°, 64.15°, and 72.14°, respectively, confirming the rhombohedral iron structure of the sample (PDF card No. 01–084-0307). Fig. 6 displays the SEM image of the leach residue from the validation experiment. The presence of Fe, as well as small amounts of Nd and Pr, was detected with EDS analysis. The results matched those obtained by ICP analysis. The SEM analysis showed that the leach residue consisted of large particles.

The EDS study revealed the presence of Fe and minor amounts of Nd and Pr. The SEM analysis revealed that the leach residue was composed of large particles. The FT-IR spectra of the leach residue from the validation experiment and stretching region are illustrated in Fig. 7.

Table 5 illustrates the tabulated FTIR data and corresponding references.

The FT-IR spectra of the leach residue was recorded in the wavenumber range of 400–4000 cm^{-1} in ambient atmosphere. Fig. 7 illustrates the FT-IR spectra as well as the stretching regions. The IR spectra of the leach residue shows two minor peaks at 564 and 677 cm^{-1} in the far-IR range. The stretching vibrational mode of metal (Fe—O) oxygen bonding is responsible for the peaks at 564 cm^{-1} and 677 cm^{-1}. The Fe-O-H stretching vibrational mode generates two small peaks at 819 cm^{-1} and 1040 cm^{-1}. The high intense band identified at 1321.51 cm^{-1} is associated with the O—H stretching. The broadest band is found in the

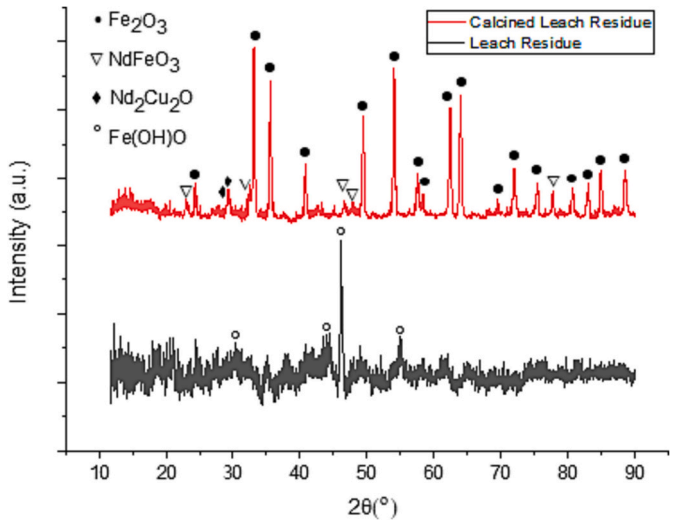

Fig. 5. XRD analysis of the as-filtered and calcined leach residue from the validation experiment.

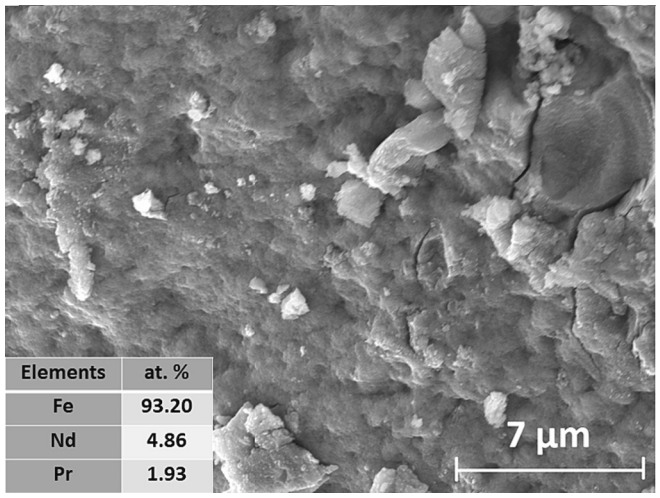

Fig. 6. SEM images of the leach residue from validation experiment at 10,000X magnification.

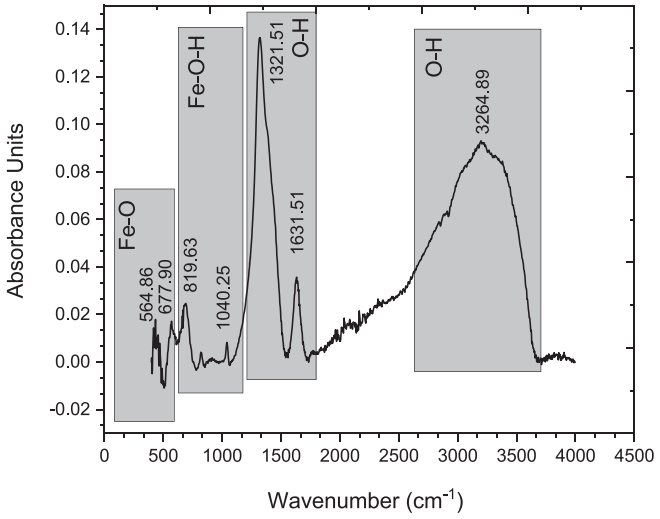

Fig. 7. FT-IR spectra of the leach residue from the validation experiment.

Table 5
The Tabulated FTIR Data with their references.

Wavenumber (cm^{-1})	Assignment	Reference
3264.89	O-H	(Obreja et al., 2013, Chhabra et al., 2012)
1631.51 and 1321.51	O-H	(Ţucureanu et al., 2016, Chhabra et al., 2012)
819.63 and 1040.25	Fe-O-H	(Pinto et al., 2019, Raul et al., 2012
564.86 and 677.90	Fe-O	(Pinto et al., 2019, Raul et al., 2012

Table 6
The experimental parameters for magnet leaching and the results of experiments based on Taguchi's orthogonal arrays.

Experiment Code	Molarity of Acid (mol/L)	Solid/ Liquid Ratio	Temperature (°C)	Stirring Speed (rpm)	Leaching Eff. [Fe] %	S/N for Fe (db)	Leaching Eff. [REE] %	S/N for REE (db)
D1	1	1:10	RT	200	19	14.43	23	−12.765
D2	1	1:20	40	350	50	6.02	59	−4.58
D3	1	1:30	60	500	63	4.01	79	−2.05
D4	2	1:10	40	500	10	20.26	69	−2.97
D5	2	1:20	60	200	75	2.5	78	−2.15
D6	2	1:30	RT	350	99	0.08	96	−0.35
D7	3	1:10	60	350	30	10.46	91	−0.81
D8	3	1:20	RT	500	87	1.21	84	−1.51
D9	3	1:30	40	200	93	0.63	88	−1.11

Table 7
ANOVA results for extraction of REEs.

Parameter	DoF	SS	MS	F-value	*P*-value
Acid Concentration	2	165.767	82.883	32.72	0.000*
Solid: Liquid Ratio	2	75.829	37.914	14.97	0.0014
Temperature	2	64.302	32.151	12.69	0.0024
Stirring Speed	2	71.005	35.502	14.02	0.0017
Total	17				

Table 8
ANOVA results for extraction of iron.

Parameter	DoF	SS	MS	F-value	P-value
Acid Concentration	2	39.167	19.584	7.85	0.0106
Solid: Liquid Ratio	2	582.457	291.229	116.71	0.000*
Temperature	2	17.291	8.646	3.46	0.0766
Stirring Speed	2	11.518	5.759	2.31	0.1552
Total	17	672.891			

near-IR region, extending about 2600–3650 cm^{-1}, with the second-highest strong peak at 3264 cm^{-1} corresponding to the O—H stretching vibrational mode.

3.3. Taguchi's analysis of the leaching process and statistical analysis

The three-level L9 orthogonal array was employed to optimize the leaching efficiencies of iron and REEs. Table 6 presents the leaching parameters and the level of experiments with chemical analysis determined by ICP analysis. The S/N ratio for REEs and iron were calculated with Eq. (10) (larger is better) and Eq. (11) (smaller is better), respectively. Table 6 presents the S/N ratio values for each experiment. Afterward, ANOVA analysis was used for determining the contribution of each process parameter.

$$S/N = -10log\left[\frac{1}{n}\sum_{i=1}^{n}\left(\frac{1}{y_i^2}\right)\right] \quad (10)$$

$$S/N = -10log\left[\frac{1}{n}\sum_{i=1}^{n}\left(y_i^2\right)\right] \quad (11)$$

The F-values, Mean Square (MS), and Sum Square (SS) values can be determined by statistical analysis. Table 7 and Table 8 represent the calculated values for the extraction of REEs and the dissolution of iron, respectively.

The P-value illustrates the statistical importance of the leaching parameters. Statistical analysis revealed that, while all experimental parameters are statistically important for the extraction of REEs, acid

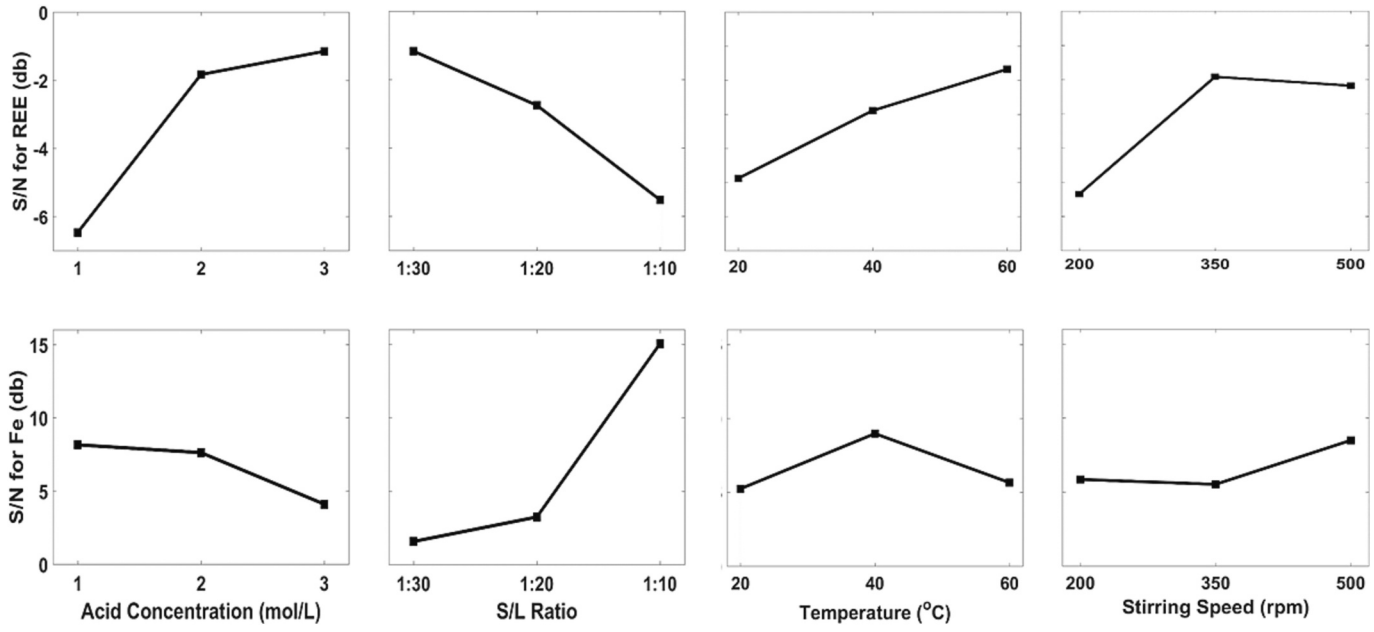

Fig. 8. The effect of the leaching parameters on the optimization criteria for both REEs and Fe.

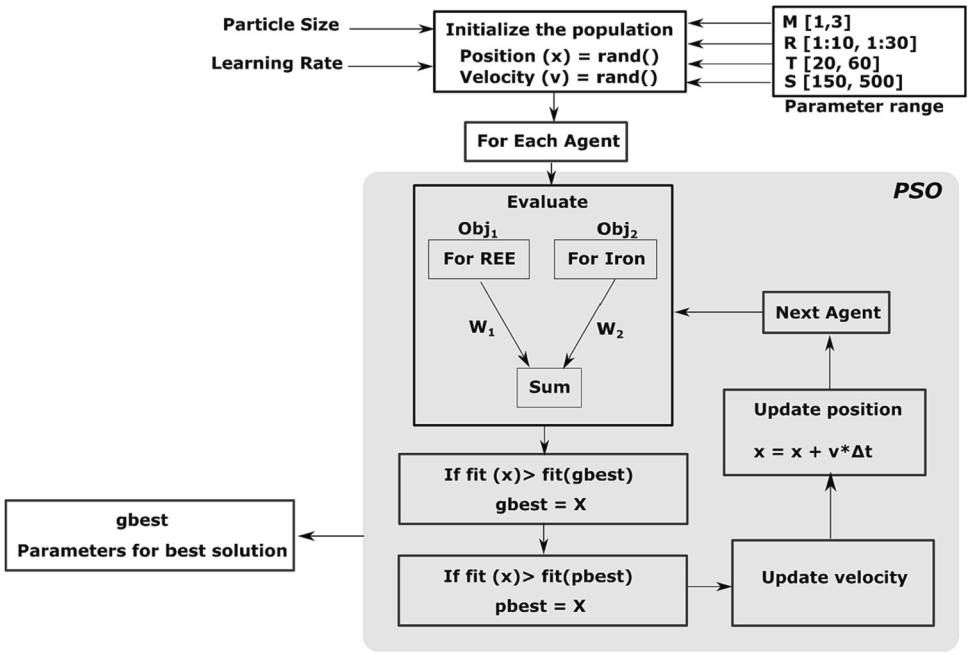

Fig. 9. Flow chart for utilizing PSO.

concentration and solid/liquid ratio are the important parameters for the extraction of iron under the experimental working conditions. Fig. 8 illustrates the effect of the leaching parameters on the optimization criteria for both REEs and Fe.

According to the Taguchi plots, NdFeB magnet powders should be leached in 3 mol/L of nitric acid solution with a solid/liquid ratio of 1:30 and a stirring speed of 350 rpm at a process temperature of 60 °C to achieve maximum REEs contents in the leach liquor. On the other hand, magnet powders should be leached in a solution of 1 mol/L of acid concentration, at a solid/liquid ratio of 1:10 and at a stirring speed of 500 rpm, at a process temperature of 60 °C to achieve minimum extraction of iron. Validations experiments were conducted under the specified experimental conditions. The leaching efficiencies of REEs and iron were 99% and 99%, respectively, under the specified conditions for maximum REEs. On the other hand, the leaching efficiencies of REEs and iron were 28% and 22%, respectively, under the specified condition for minimum iron content. The chemical analysis results are consistent with the Taguchi results. As a result of these findings, traditional precipitation steps are required for removing iron from the leach liquor. The pH value would be below 1 due to high nitric acid concentration. Adjusting the pH values is required to remove iron from the leach liquor. To achieve both maximum REEs and minimum iron extraction, particle swarm optimization method (PSO) was chosen. The particle swarm optimization was coded with the equations obtained from the regression analysis to attain both maximum REEs extraction and minimum iron extraction.

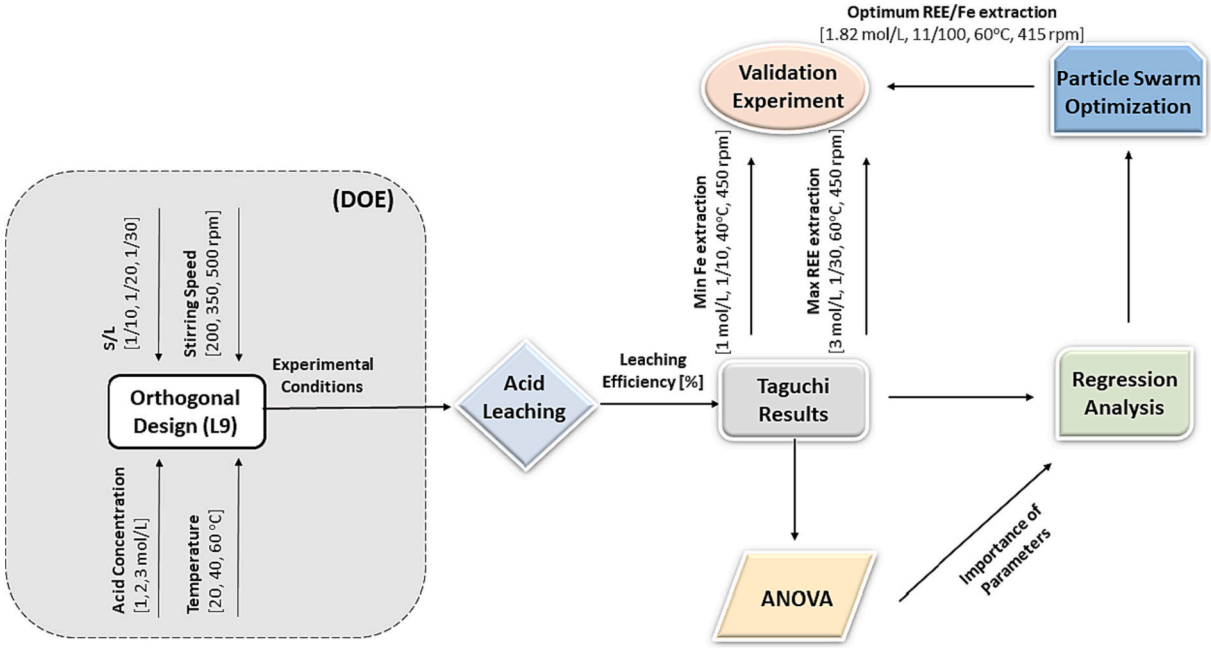

Fig. 10. Flowchart for model-supported iron minimization via in-situ hydrolysis during oxidative leaching.

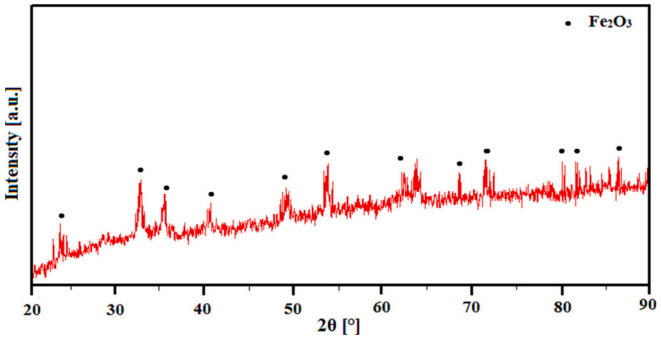

Fig. 11. XRD pattern of the precipitate in the autoclave.

3.4. Regression analysis of REEs and iron

There are two main purposes of the leaching as follows; (1) maximize the extraction of REEs and (2) minimize iron dissolution. The leaching experiments were carried out with different levels of acid concentration (M), solid-liquid ratio (R), temperature (T), and stirring speed (S) to ascertain the contribution of the experimental parameters Furthermore, it is conducted to determining the relationships between the aforementioned parameters and the output variables. The regression analysis was employed for the REEs equation, and the iron dissolution equation based on the specified input parameters. Based on the results obtained from the chemical analysis, Eq. (12) and Eq. (13) provide the computed equations for the iron dissolution and REEs extraction.

$$Fe_{dissolution} = -36.79 + 24.33M - 1.607R - 4.55M^2 + 0.032R^2 \quad (12)$$

$$REE_{extraction} = -6.06 + 9.02M - 0.84R + 0.02T + 0.02S - 3.42M^2 + 0.118R^2 + 0.055T^2 - 0.0025S^2 \quad (13)$$

Eq. (12) shows the regression equation for iron dissolution which has $R^2 = 96.08\%$, $R^2 - adjusted = 92.32\%$, and $R^2 - predict = 79.29\%$. Eq. (13) shows the regression equation for the extraction of REEs which has $R^2 = 96.91\%$, $R^2 - adjusted = 93.93\%$, and $R^2 - predict = 75.72\%$. The term R^2 is a statistical indicator of how closely the data match the regression line that was fitted. Moreover, the R^2-adjusted value presents model accuracy and R^2. The R^2 values in this study indicate the models are a good fit. Determining the lowest and maximum values of these equations, respectively, requires multi-objective optimization which defines the input parameters.

Table 9
Box-Behnken matrix and the results concerning the percentage of iron and REEs content in the leach liquor after iron precipitation in the autoclave.

Sample	Process Temperature [°C]	Time [h]	Water Addition [vol%]	Recovery Eff. of REEs %	Removal Eff. of Iron %
A1	120	2	25	89	1
A2	160	2	25	47	0.06
A3	120	6	25	72	0.7
A4	160	6	25	21	0.06
A5	120	4	0	71	0.3
A6	160	4	0	31	0.05
A7	120	4	50	80	1.7
A8	160	4	50	40	0.1
A9	140	2	0	56	0.4
A10	140	6	0	52	0.05
A11	140	2	50	62	1
A12	140	6	50	41	0.1
A13	140	4	25	82	0.07
A14	140	4	25	79	0.04
A15	140	4	25	83	0.05

Table 10
ANOVA results for REEs precipitation.

Source	DF	Adj SS	Adj MS	F-Value	P-Value
Model	9	6117.18	679.69	24.91	0.001
Linear	3	4340.25	1446.75	53.03	0.000
Temperature	1	3741.13	3741.13	137.12	0.000*
Time	1	578.00	578.00	21.19	0.006
Water Addition	1	21.13	21.13	0.77	0.419
Square	3	1684.43	561.48	20.58	0.003
Temperature*Temperature	1	420.10	420.10	15.40	0.011
Time*Time	1	664.64	664.64	24.36	0.004
Water Addition* Water Addition	1	849.33	849.33	31.13	0.003
2-Way Interaction	3	92.50	30.83	1.13	0.421
Temperature*Time	1	20.25	20.25	0.74	0.428
Temperature* Water Addition	1	0.00	0.00	0.00	1.000
Time* Water Addition	1	72.25	72.25	2.65	0.165
Error	5	136.42	27.28		
Lack-of-Fit	3	127.75	42.58	9.83	0.094
Pure Error	2	8.67	4.33		
Total	14	6253.60			

3.5. Optimization of the leaching process

This study aims to identify the optimal leaching parameters both for minimizing iron through in-situ iron hydrolysis and for maximizing REEs extraction during the leaching process. Particle swarm optimization (PSO) has been effective in order to optimize difficult multifunctional and dimensional discontinuous problems (Eberhart and Shi, 1998). The PSO is a nature-inspired optimization method, which needs neither any mathematical relation nor pre-processing. Moreover, it can be easily implemented since it is based on the swarm technique. To find max/min points, it utilizes the intelligence and movement of the particles. Moreover, it is a robust stochastic evolutionary computational technique (Robinson and Rahmat-Samii, 2004). The other optimization techniques are compared with PSO elsewhere (Tharwat and Schenck,

Table 11
ANOVA results for iron precipitation.

Source	DF	Adj SS	Adj MS	F-Value	P-Value
Model	9	3.31798	0.36866	9.11	0.013
Linear	3	2.32218	0.77406	19.12	0.004
Temperature	1	1.47061	1.47061	36.33	0.002
Time	1	0.30031	0.30031	7.42	0.042
Water Addition	1	0.55125	0.55125	13.62	0.014
Square	3	0.44206	0.14735	3.64	0.099
Temperature*Temperature	1	0.28093	0.28093	6.94	0.046
Time*Time	1	0.05846	0.05846	1.44	0.283
Water Addition* Water Addition	1	0.16026	0.16026	3.96	0.103
2-Way Interaction	3	0.55375	0.18458	4.56	0.068
Temperature*Time	1	0.02250	0.02250	0.56	0.489
Temperature* Water Addition	1	0.45562	0.45562	11.26	0.020
Time* Water Addition	1	0.07563	0.07563	1.87	0.230
Error	5	0.20239	0.04048		
Lack-of-Fit	3	0.20192	0.06731	288.46	0.003
Pure Error	2	0.00047	0.00023		
Total	14	3.52037			

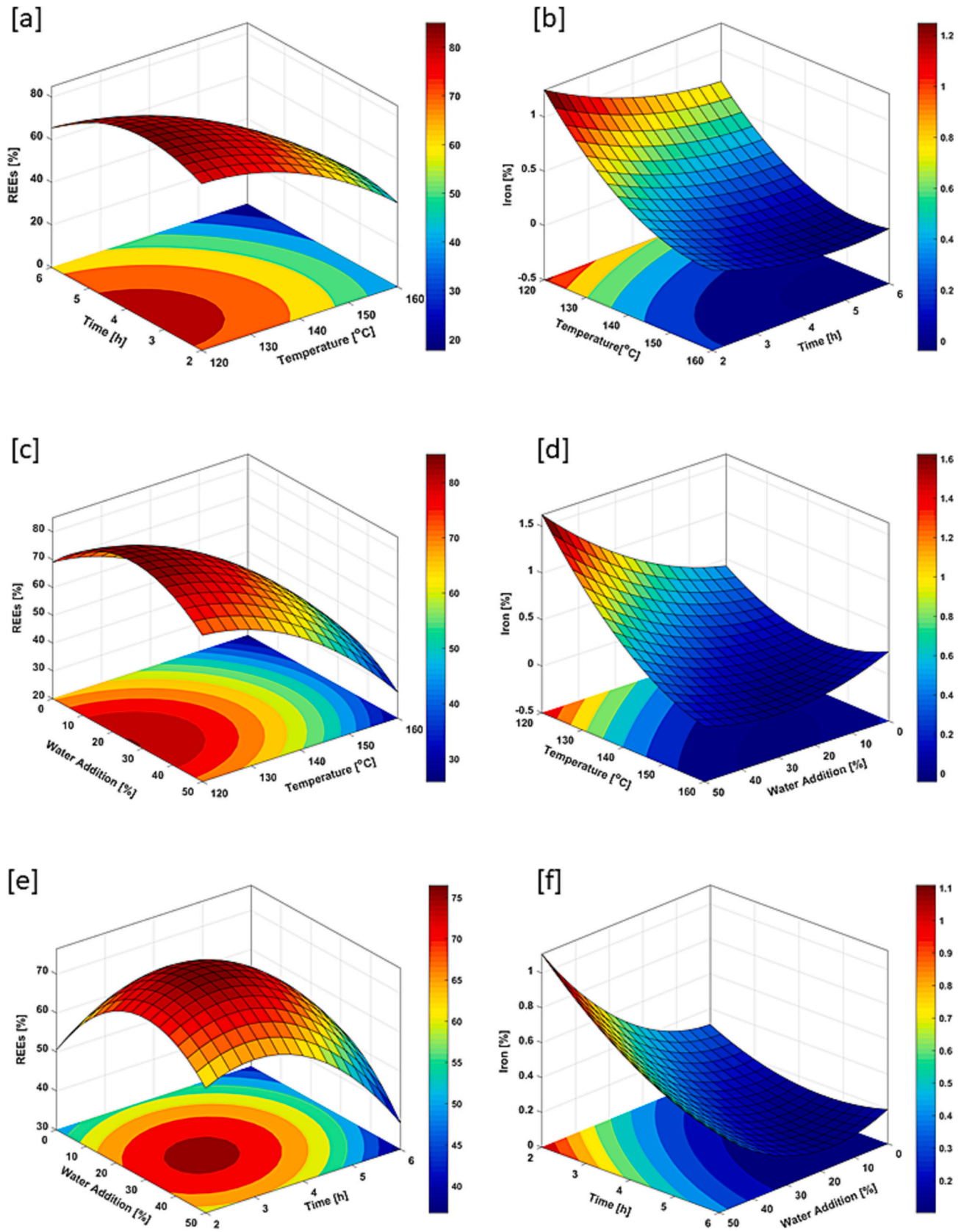

Fig. 12. (a), (c), (e) and (b(, (d), (f) represent the response surface plots for iron precipitation and REEs, respectively.

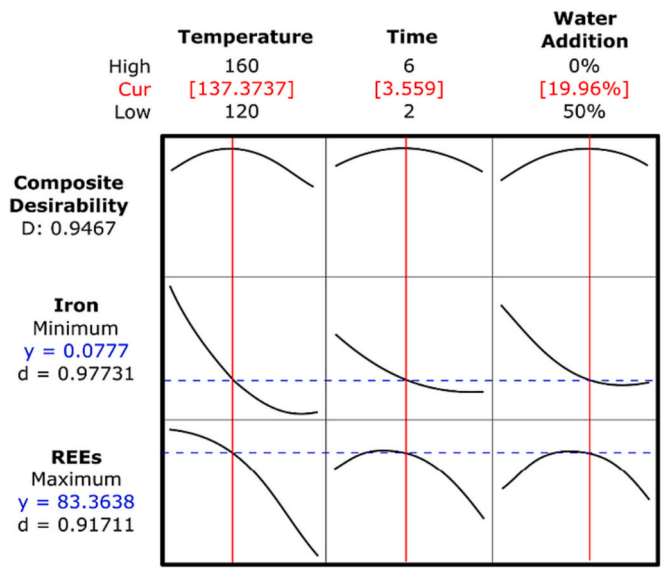

Fig. 13. Optimization plots for maximum REEs and minimum iron content in the leach liquor.

2021; Khan and Sahai, 2012). Hence, optimization algorithms based on nature-inspired are suggested for difficult multidimensional discontinuous systems. Apart from these, this algorithm allows combining and hybridizing for improving the performance of the common algorithms. Therefore, the PSO method was chosen both for maximizing REEs extraction and for minimizing iron extraction.

Based on the regression analysis, Eq. (12) and (13) are defined as the target function for the multi-objective function of the PSO. The multi-objective function in Eq. (1) has two goals: (1) maximizing the extraction of REEs and (2) minimizing iron extraction.

$$Recycling_{obj} = min(w_1(|REE(M,R,T,S) - g_1|) + w_2(|Fe(M,R,T,S) - g_2|)), -1 < w_1 < 0 < w_2 < 1 \quad (14)$$

Here in Eq. 14, −1 is given as a negative sign to maximize the efficiency of REEs extraction. On the other hand, 1 is described as a positive sign to reduce iron extraction efficiency.

The values 100 and 0 belong to the values of g_1 and g_2, respectively. For PSO, input parameter constraints, inertia, learning factor, iteration number, and particle size must also be defined. Fig. 9 depicts a flowchart for the application of the multi-objective PSO algorithm.

As a result of the PSO, the optimal parameters were found to be an acid concentration of 1.82 mol/L, a solid/liquid ratio of 11/100, a process temperature of 60 °C, and a stirring speed of 415 rpm. Under these specified conditions, 84% of REEs and 5% of iron would be dissolved during the oxidative leaching process. Validation studies with the specified conditions were carried out 10 times. The mean REEs and iron leaching efficiencies were calculated to be 76% and 7%, respectively. These results are good since such low iron extraction in any of the baseline experiments was not achieved. Fig. 10 displays a flowchart for model-supported iron minimization via in-situ hydrolysis during the oxidative leaching.

3.6. Characterization of the precipitate formed in the autoclave

The precipitation of hematite from the leach liquor under pressure and a high temperature was performed. A nitric acid medium offers highly oxidizing conditions and the use of oxygen directly from the air, thus Fe^{3+} is generated in the leach liquor. In this study, Fe^{3+} was hydrolyzed to hematite under pressure and a high temperature. The hydrolysis reaction of Fe^{3+} to hematite is given in the following Eq. (15):

$$2Fe^{3+} + 6NO_3^- + 3H_2O = Fe_2O_3 + 6HNO_3 \quad (15)$$

The precipitation of hematite at approximately 137 °C from leach liquor was performed in an autoclave under pressure for four hours to remove the remaining iron after the leaching process. High purity (98%) REEs in leach liquor was achieved after the hematite precipitation. The precipitate was characterized by XRD analysis. Fig. 11 shows the XRD pattern of hematite.

The XRD peaks were indexed by the rhombohedral phase of Fe_2O_3 with a standard pattern from (JCPDS) file no 84–0307.

3.7. Iron precipitation under pressure and high temperature

Moreover, investigating the effect and combined effect of each process parameter requires several experiments conducted based on the Box-Behnken design. The significant experimental parameters affecting the efficiency of iron removal under pressure and temperature in the autoclave were determined by ANOVA analysis.

The precipitation process was optimized with the RSM, which results in minimum iron and maximum REEs contents in the leach liquor. Table 9 shows the Box-Behnken matrix and the results concerning the percentage of iron and REEs content in the leach liquor after iron precipitation in the autoclave.

3.8. Model fitting, statistical analysis, and response surface analysis

The empirical relationship between the input parameters (temperature T, time TM, and water addition W) and the output variables were examined through regression analysis. The equations for the precipitation of REEs and iron are given in Eq. (16) and Eq. (17), respectively.

$$REEs = -464 + 6.61\,T + 24.1\,TM + 16.18\,W - 0.02667\,T{*}T - 3.354\,TM{*}TM - 0.607\,W{*}W - 0.0562\,T{*}TM - 0.0000\,T{*}W + 0.425\,TM{*}W \quad (16)$$

$$Fe = 29.09 - 0.2726\,T - 0.817\,TM - 0.830\,W + 0.000690\,T{*}T + 0.0315\,TM{*}TM + 0.00833\,W{*}W + 0.00187\,T{*}TM + 0.00338\,T{*}W + 0.0137\,TM{*}W \quad (17)$$

The regression equation for the precipitation of REEs is given in Eq. (16), with R^2 = 94.25% and R^2-adjusted = 83.90%. Additionally, Eq. (17) gives the regression equation with R^2 = 97.82% and R^2-adjusted = 93.89% for the iron precipitation. The R^2 value is a statistical indicator of how closely the data match the regression line that was fitted. Moreover, the R^2-adjusted value presents model accuracy and R^2. The R^2 values in this study indicate the models are a good fit. Table 10 and Table 11 show the findings of the ANOVA analysis. The F-value for each parameter shows how each precipitation parameter affects the purity of solution. A *P*-value of <0.05 indicates the statistical significance of each process parameter. The MS, SS, F-value, and the P-value of the process parameters are shown in Tables 10 and 11, respectively, for REEs and iron.

Statistical analysis revealed that, while temperature and time are important parameters for the precipitation of REEs, temperature, time and water addition are the significant parameters for the removal of iron in the autoclave under the experimental working conditions.

Fig. 12 presents the response surface plots for the relationship between temperature, time, and the addition of water to the removal of

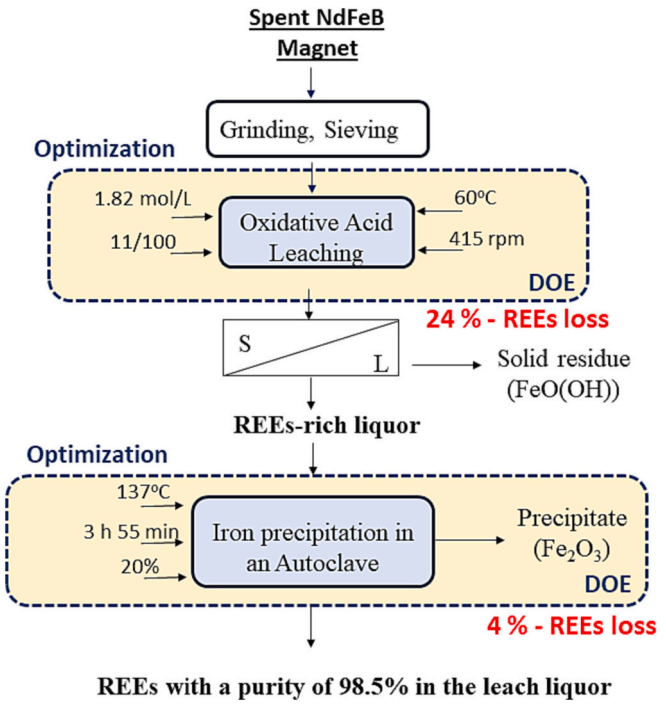

Fig. 14. The proposed conceptual flowsheet for high REEs recovery from spent NdFeB magnets.

iron. Fig. 12 (a), (c), (e) and 4.27 (b), (d), (f) represent the response surface plots for iron precipitation and REEs, respectively.

For the NdFeB magnets recycling, the main purpose is to achieve the high purity of REEs. Therefore, the efficiency of the REEs recovery is needed to be increased using defining optimal input parameters without losing REEs.

Fig. 12 (a) illustrates the surface response and contour plots for determining the maximum REEs content and the minimum iron content in the leach liquor. A process time of <4.5 h and a temperature of <130 °C provide the maximum REEs content in the leach liquor after the autoclave experiment. On the other hand, Fig. 12 (b) shows the effect of temperature and time on iron precipitation. This figure also illustrates that iron removal can be achieved when the time is longer than 4 h and the temperature is higher than 150 °C. The combination of water addition and temperature was studied for the REEs and iron content in the leach liquor. Fig. 12 (c) displays the maximum content of REEs in the leach liquor achieved at low temperatures and at a water addition of between 25% and 30%. Furthermore, the effect of these process parameters on iron removal is illustrated in Fig. 12 (d). This figure also demonstrates that the maximum iron removal is observed at a process temperature of about 160 °C and water addition of between 20% and 40%. The effects of water addition and process time for REEs and iron are presented in Fig. 12 (e) and (f), respectively. These figures indicate that the purity of the leach liquor can be increased at high-temperature values and low water addition. However, high REEs content in the leach liquor were obtained for the period of 2.5 h < TM < 4.5 h and at water addition of 25% < W < 35%, as shown in Fig. 12 (e). These surface response and contour plots show that temperature is defined as the most important parameter for the promising results of the iron removal process. This conclusion is also consistent with the ANOVA results for the iron removal process in the autoclave.

3.9. Optimization of the iron precipitation process in the autoclave

This optimization process aims to achieve high-purity REEs in the leach liquor while the precipitation of REEs together with iron is prevented. Therefore, both a maximum REEs content and a minimum iron content are anticipated during the iron removal process in the autoclave. For this purpose, an optimization study was conducted with MINITAB. The optimization plot for both maximum REEs and minimum iron contents is presented in Fig. 13.

The optimal parameters were determined to be a process

Table 12
REEs recovery and iron removal efficiencies.

	REEs recovery efficiency (%)		
NdFeB magnet powders	Leaching	Precipitation	Total
	76	96	72.96
NdFeB magnet powders	**Iron removal efficiency (%)**		
	Leaching	Precipitation	Total
	93	100	100

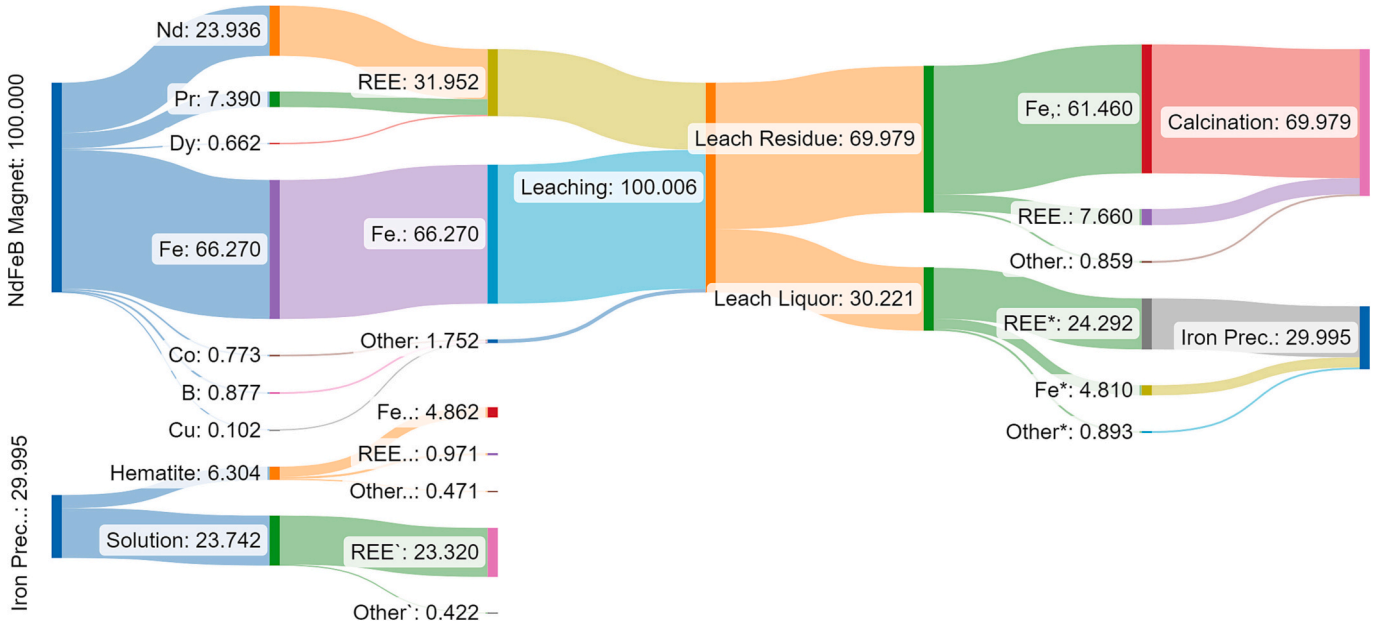

Fig. 15. Material flow analysis (MFA) for recycling of NdFeB magnets under the optimum experimental conditions.

temperature of approximately 137 °C, a process time of approximately 3 h and 55 min, and a water addition of approximately 20%. A validation experiment was conducted with these process parameters. The contents of REEs and iron in the residual leach liquor were calculated to be 96% and 0.1%, respectively. Thus, iron was removed from the system with a 4% loss of REEs.

Compared to the direct leaching of the magnet powders, the proposed conceptual flowsheet for the recovery of REEs ensures extraction of REEs selectively during the leaching experiments. Moreover, the following step for the iron removal process in an autoclave proved effective for obtaining high-purity REEs in the leach liquor. Advantages of this flowsheet include a high REEs recovery efficiency and the precipitation of the hematite without the need for adding a precipitation agent. Fig. 14 illustrates the proposed conceptual flowsheet for high REEs recovery from spent NdFeB magnets.

Fig. 15 illustrates a material flow analysis (MFA) for the recycling of NdFeB magnets under the optimum experimental conditions. All flows are in percentage.

The overall mass flows obtained from the chemical analysis are shown by the Sankey diagram (Fig. 15). The REEs flow starts on the left side of the diagram with 31.95% and 24% of REEs lost during oxidative leaching. After the iron precipitation in the autoclave, approximately 76% of REEs are recovered under the optimum conditions, with >98% purity achieved.

Table 12 presents the REEs recovery and iron removal efficiencies.

The REE recovery efficiencies are 76% and 96% in the leaching and the precipitation stages, respectively. Iron removal efficiencies are 93% and 100% in the leaching and the precipitation stages, respectively.

4. Conclusion

In this study, iron dissolution was avoided throughout the leaching process through in-situ iron hydrolysis. Afterward, the dissolved iron was precipitated in the autoclave with the aim of removal of iron from the system. Notable findings of this study are given as follows;

- Taguchi method was employed to determine the optimal leaching parameters for maximum REEs extraction and minimum iron extraction. Afterward, PSO was computed to define optimum leaching parameters. Based on the average ten validation leaching experiments, leaching efficiencies of REEs and iron were 76% and 7%, respectively.
- Statistical analysis revealed that, while solid/liquid ratio is the most important parameter for minimizing iron extraction under experimental working conditions, acid concentration, and solid/liquid ratio are important parameters for maximizing REEs extraction.
- The optimization tool in MINITAB gives the optimum parameters for the minimum iron and maximum REEs content in the leach liquor. The validation experiment was performed at a process temperature of approximately 137 °C, a processing time of about 3 h 55 min, and a water addition of approximately 20%. Under the specified experimental conditions, the contents of REEs and iron in the residual leach liquor were calculated to be 96% and 0.1%, respectively. Thus, iron was removed from the system with a 4% of REEs loss.
- Statistical analysis shows that, while temperature and time are important parameters for the precipitation of REEs, temperature, time and water addition are the significant parameters for the precipitation of iron in the autoclave.

Author contributions

Conceptualization E.E.K. and B.F., Experiments, E.E.K, Data curation E.E.K, O.K. Formal analysis E.E.K, O.K. Funding acquisition S·S, S.G, B. F., Investigation E.E.K., Methodology E.E.K and O.K. Project Administration S·S, S.G, B.F., Resources B.F., Supervision B.F. and S.G., *V*alidation E.E.K, Writing-original draft E.E.K, and O.K. writing-review % editing E.E.K., and B.F.

Declaration of Competing Interest

The authors declare that they have no known competing financial interests or personal relationships that could have appeared to influence the work reported in this paper.

Acknowledgments

This research was funded by Federal Ministry for Economic Affairs and Climate Action, Germany grant number 287 EN (Project “Sustainable recovery of rare earth elements (Nd, Pr, Dy) from spent magnets”). The authors would like to greatly acknowledge The Scientific of Technological Research Council of Turkey under grant agreement 120N331 for financial support.

References

Akcil, A., Ibrahim, Y.A., Meshram, P., Panda, S., Abhilash, 2021. Hydrometallurgical recycling strategies for recovery of rare earth elements from consumer electronic scraps: a review. J. Chem. Technol. Biotechnol. 96 (7), 1785–1797. https://doi.org/10.1002/jctb.6739.

Babjan, C., 1971. Synthesis of jarosite—KFe3(SO4)2(OH)6. Geol. Zb. pp. 22 (2), 299–304.

Barkov, A.Y., Sharkov, E.V., Nikiforov, A.A., Korolyuk, V.N., Silyanov, S.A., Lobastov, B. M., 2021. Compositional variations of apatite and REE-bearing minerals in relation to crystallization trends in the monchepluton layered complex (Kola peninsula). Russ. Geol. Geophys. 62 (4), 427–444. https://doi.org/10.2113/RGG20194055.

Böhm, D., Czerski, K., Gottlieb, S., Huke, A., Ruprecht, G., 2023. Recovery of rare earth elements from NdFeB magnets by chlorination and distillation. Processes 11 (2), 577. https://doi.org/10.3390/pr11020577.

Cheng, T.C., Demopoulos, G.P., 2004. Hydrolysis of ferric sulfate in the presence of zinc sulfate at 200 C: precipitation kinetics and product characterization. Ind. Eng. Chem. Res. 43 (20), 6299–6308. https://doi.org/10.1021/ie030711g.

Cheng, T.C., Demopoulos, G.P., Shibachi, Y., Masuda, H., 2003. The precipitation chemistry and performance of the Akita hematite process—an integrated laboratory and industrial scale study. Electrometall. and environment. Hydrometall. 2, 1657–1674. https://doi.org/10.1002/9781118804407.ch44.

Chhabra, V.A., Deep, A., Kaur, R., Kumar, R., 2012. Functionalization of graphene using carboxylation process. Int. J. Sci. Emerg. Technol. with Latest Trends 4, 13–19.

Chung, H., Stopic, S., Emil-Kaya, E., Gürmen, S., Friedrich, B., 2022. Recovery of rare earth elements from spent NdFeB-magnets: separation of iron through reductive smelting of the oxidized material (second part). Metals 12 (10), 1615. https://doi.org/10.3390/met12101615.

Coello, C.A.C., Pulido, G.T., Lechuga, M.S., 2004. Handling multiple objectives with particle swarm optimization. IEEE Trans. Evol. 8 (3), 256–279. https://doi.org/10.1109/TEVC.2004.826067.

Dahasahastra, A.V., Balasundaram, K., Latkar, M.V., 2022. Turbidity removal from synthetic turbid water using coagulant recovered from water treatment sludge: a potential method to recycle and conserve aluminium. Hydrometallurgy 213, 105939. https://doi.org/10.1016/j.hydromet.2022.105939.

Du, C., Ma, S., Xie, M., Yang, F., Zhao, Z., Chen, Y., Ma, Y., 2023. Recovery of high-value rare earth elements from waste NdFeB by the water-soluble ammonium salt [Hbet] cl. Sep. Purif. Technol. 308, 122946. https://doi.org/10.1016/j.seppur.2022.122946.

Dutrizac, J.E., Riveros, P.A., 1999. The precipitation of hematite from ferric chloride media at atmospheric pressure. Metall. Mater. Trans. B Process Metall. Mater. Process. Sci. 30 (6), 993–1001. https://doi.org/10.1021/ie030711g.

Dutta, S., Mukhopadhyay, S., Gaddam, S., Shenoy, K.T., Mirji, K.V., 2021. Process development for the separation of niobium and tantalum from fluoride medium using trioctyl amine and application of Taguchi’s method to optimize solvent extraction parameters. Hydrometallurgy 199, 105522. https://doi.org/10.1016/j.hydromet.2020.105522.

Eberhart, R.C., Shi, Y., 1998. Evolving artificial neural networks. In: Proceedings of the International Conference on Neural Networks and Brain (Vol. 1, No. 998, pp. PL5-PLI3). PRC.

Emil-Kaya, E., Stopic, S., Gürmen, S., Friedrich, B., 2022. Production of rare earth element oxide powders by solution combustion: a new approach for recycling of NdFeB magnets. RSC Adv. 12 (48), 31478–31488. https://doi.org/10.1039/D2RA05876F.

Emil-Kaya, E., Polat, B., Stopic, S., Gürmen, S., Friedrich, B., 2023. Recycling of NdFeB magnets employing oxidation, selective leaching, and iron precipitation in an autoclave. RSC Adv. 13 (2), 1320–1332. https://doi.org/10.1039/D2RA06883D.

Feitknecht, V.W., Michaelis, W., 1962. Über die Hydrolyse von Eisen (III)-perchlorat-Lösungen. Helv. Chim. Acta 45 (1), 212–224. https://doi.org/10.1002/zaac.19754170207.

Ilatovskaia, M., Lonski, O., Löffler, M., Blenau, L., Charitos, A., Fabrichnaya, O., 2023. Phase relations in the CaO-Nd2O3-Al2O3 system in application for rare earth recycling. JOM 1–10. https://doi.org/10.1007/s11837-023-05731-8.

Kaya, E.E., Kaya, O., Stopic, S., Gürmen, S., Friedrich, B., 2021. NdFeB magnets recycling process: an alternative method to produce mixed rare earth oxide from scrap NdFeB magnets. Metals 11 (5), 716. https://doi.org/10.3390/met11050716.

Khan, K., Sahai, A., 2012. A comparison of BA, GA, PSO, BP and LM for training feed forward neural networks in e-learning context. Int. J. Intell. Syst. Appl. 4 (7), 23. https://doi.org/10.5815/ijisa.2012.07.03.

Kruse, S., Raulf, K., Pretz, T., Friedrich, B., 2017. Influencing factors on the melting characteristics of NdFeB-based production wastes for the recovery of rare earth compounds. J. Sustain. Metall. 3 (1), 168–178. https://doi.org/10.1007/s40831-016-0093-1.

Lewicka, E., Guzik, K., Galos, K., 2021. On the possibilities of critical raw materials production from the EU's primary sources. Resources 10 (5), 50. https://doi.org/10.3390/resources10050050.

Lin, X., Qu, Z., Chen, Y., Jin, R., Su, T., Yu, Y., Wang, Z., 2019. A novel application of hematite precipitation for high effective separation of Fe from Nd-Fe-B scrap. Sci. Rep. 9 (1), 1–8. https://doi.org/10.1038/s41598-019-54896-3.

Mudali, U.K., Patil, M., Saravanabhavan, R., Saraswat, V.K., 2021. Review on E-waste recycling: part II—Technologies for recovery of rare earth metals. Trans Indian Natl. Acad. Eng 1–19. https://doi.org/10.1007/s41403-021-00231-0.

Obreja, A.C., Cristea, D., Gavrila, R., Schiopu, V., Dinescu, A., Danila, M., Comanescu, F., 2013. Isocyanate functionalized graphene/P3HT based nanocomposites. Appl. Surf. Sci. 276, 458–467. https://doi.org/10.1016/j.apsusc.2013.03.117.

Omodara, L., Pitkäaho, S., Turpeinen, E.M., Saavalainen, P., Oravisjärvi, K., Keiski, R.L., 2019. Recycling and substitution of light rare earth elements, cerium, lanthanum, neodymium, and praseodymium from end-of-life applications-A review. J. Clean. Prod. 236, 117573. https://doi.org/10.1016/j.jclepro.2019.07.048.

Önal, M.A.R., Borra, C.R., Guo, M., Blanpain, B., Van Gerven, T., 2017. Hydrometallurgical recycling of NdFeB magnets: complete leaching, iron removal and electrolysis. J. Rare Earths 35 (6), 574–584. https://doi.org/10.1016/S1002-0721(17)60950-5.

Pan, J., Nie, T., Hassas, B.V., Rezaee, M., Wen, Z., Zhou, C., 2020. Recovery of rare earth elements from coal fly ash by integrated physical separation and acid leaching. Chemosphere 248, 126112. https://doi.org/10.1016/j.chemosphere.2020.126112.

Parhi, P.K., Sethy, T.R., Rout, P.C., Sarangi, K., 2016. Separation and recovery of neodymium and praseodymium from permanent magnet scrap through the hydrometallurgical route. Sep. Sci. Technol. 51 (13), 2232–2241. https://doi.org/10.1080/01496395.2016.1200087.

Peelman, S., Sun, Z.H., Sietsma, J., Yang, Y., 2016. Leaching of rare earth elements: review of past and present technologies. J. Rare Earths 319–334. https://doi.org/10.1016/B978-0-12-802328-0.00021-8.

Pinto, P.S., Lanza, G.D., Ardisson, J.D., Lago, R.M., 2019. Controlled dehydration of Fe (OH) 3 to Fe 2 O 3: developing mesopores with complexing iron species for the adsorption of β-lactam antibiotics. J. Braz. Chem. Soc. 30, 310–317. https://doi.org/10.21577/0103-5053.20180179.

Polyakov, E.G., Sibilev, A.S., 2015. Recycling rare-earth-metal wastes by pyrometallurgical methods. Metallurgist 59 (5), 368–373. https://doi.org/10.1007/s11015-015-0111-8.

Rabatho, J.P., Tongamp, W., Takasaki, Y., Haga, K., Shibayama, A., 2013. Recovery of Nd and Dy from rare earth magnetic waste sludge by hydrometallurgical process. J. Mater. Cycles Waste Manag. 15 (2), 171–178. https://doi.org/10.1007/s10163-012-0105-6.

Raul, P.K., Devi, R.R., Umlong, I.M., Banerjee, S., Singh, L., Purkait, M., 2012. Removal of fluoride from water using iron oxide-hydroxide nanoparticles. J. Nanosci. Nanotechnol. 12 (5), 3922–3930. https://doi.org/10.1166/jnn.2012.5870.

Rim, K.T., 2016. Effects of rare earth elements on the environment and human health: a literature review. J. Toxicol. Environ. 8 (3), 189–200. https://doi.org/10.1007/s13530-016-0276-y.

Riveros, P.A., Dutrizac, J.E., 1997. The precipitation of hematite from ferric chloride media. Hydrometallurgy 46 (1–2), 85–104. https://doi.org/10.1016/S0304-386X(97)00003-0.

Robinson, J., Rahmat-Samii, Y., 2004. Particle swarm optimization in electromagnetics. IEEE Trans. Antennas Propag. 52 (2), 397–407. https://doi.org/10.1109/TAP.2004.823969.

Stopic, S., Polat, B., Chung, H., Emil-Kaya, E., Smiljanić, S., Gürmen, S., Friedrich, B., 2022. Recovery of rare earth elements through spent NdFeB magnet oxidation (first part). Metals 12 (9), 1464. https://doi.org/10.3390/met12091464.

Tay, S.L., Scott, J.M., Palmer, M.C., Reid, M.R., Stirling, C.H., 2021. Occurrence, geochemistry and provenance of REE-bearing minerals in marine placers on the west coast of the South Island, New Zealand. N. Z. J. Geol. 64 (1), 89–106. https://doi.org/10.1080/00288306.2020.1736585.

Tharwat, A., Schenck, W., 2021. A conceptual and practical comparison of PSO-style optimization algorithms. Expert Syst. Appl. 167, 114430. https://doi.org/10.1109/TAP.2004.823969.

Tian, Y., Liu, Z., Zhang, G., 2019. Recovering REEs from NdFeB wastes with high purity and efficiency by leaching and selective precipitation process with modified agents. J. Rare Earths 37 (2), 205–210. https://doi.org/10.1016/j.jre.2018.10.002Get rights and content.

Ţucureanu, V., Matei, A., Avram, A.M., 2016. FTIR spectroscopy for carbon family study. Crit. Rev. Anal. Chem. 46 (6), 502–520. https://doi.org/10.1080/10408347.2016.1157013.

Tunsu, C., Petranikova, M., Ekberg, C., Retegan, T., 2016. A hydrometallurgical process for the recovery of rare earth elements from fluorescent lamp waste fractions. Sep. Purif. Technol. 161, 172–186. https://doi.org/10.1016/j.seppur.2016.01.048.

Unal, F., Kaya, F., 2020. Modelling of relation between synthesis parameters and average crystallite size of Yb2O3 nanoparticles using box-Behnken design. Ceram. Int. 46 (17), 26800–26808. https://doi.org/10.1016/j.ceramint.2020.07.155.

Uysal, E., Al, S., Emil-Kaya, E., Stopic, S., Gürmen, S., Friedrich, B., 2022. Hydrometallurgical recycling of waste NdFeB magnets: design of experiment, optimisation of low concentrations of sulphuric acid leaching and process analysis. Can. Metall. Q. 1-12 https://doi.org/10.1080/00084433.2022.2058152.

Venkatesan, P., Sun, Z.H.I., Sietsma, J., Yang, Y., 2018. An environmentally friendly electro-oxidative approach to recover valuable elements from NdFeB magnet waste. Sep. Purif. Technol. 191, 384–391. https://doi.org/10.1016/j.seppur.2017.09.053.

Wang, K., Li, J., McDonald, R.G., Browner, R.E., 2011. The effect of iron precipitation upon nickel losses from synthetic atmospheric nickel laterite leach solutions: statistical analysis and modelling. Hydrometallurgy 109 (1–2), 140–152. https://doi.org/10.1016/j.hydromet.2011.06.009.

Yazici, E.Y., Deveci, H., 2013. Extraction of metals from waste printed circuit boards (WPCBs) in H2SO4–CuSO4–NaCl solutions. Hydrometallurgy. 139, 30–38. https://doi.org/10.1016/j.hydromet.2013.06.018.

Zhang, Y., Gu, F., Su, Z., Liu, S., Anderson, C., Jiang, T., 2020a. Hydrometallurgical recovery of rare earth elements from NdFeB permanent magnet scrap: a review. Metals 10 (6), 841. https://doi.org/10.3390/met10060841.

Zhang, W., Lin, Y.C., Chien, S.K., Wu, T.Y., Chen, S.C., Cheng, P.C., Lai, C.N., 2020b. Efficient indium leaching and recovery from waste liquid crystal displays panels using microwave and ultrasound-assisted heating system. Sep. Purif. Technol. 250, 117154. https://doi.org/10.1016/j.seppur.2020.117154.